Volume 1 | Number 1 | Jan 2013 | Pages 1–100

Chemical Science

www.rsc.org/chemicalscience

ROYAL SOCIETY OF CHEMISTRY

This is an *Accepted Manuscript*, which has been through the Royal Society of Chemistry peer review process and has been accepted for publication.

Accepted Manuscripts are published online shortly after acceptance, before technical editing, formatting and proof reading. Using this free service, authors can make their results available to the community, in citable form, before we publish the edited article. We will replace this *Accepted Manuscript* with the edited and formatted *Advance Article* as soon as it is available.

You can find more information about *Accepted Manuscripts* in the **Information for Authors**.

Please note that technical editing may introduce minor changes to the text and/or graphics, which may alter content. The journal's standard **Terms & Conditions** and the **Ethical guidelines** still apply. In no event shall the Royal Society of Chemistry be held responsible for any errors or omissions in this *Accepted Manuscript* or any consequences arising from the use of any information it contains.

Journal Name

ARTICLE

Organic Solid Fluorophores Regulated by Subtle Structure Modification: Color-Tunable and Aggregation-Induced Emission

Jing Nan Zhang,[a‡] Hui Kang,[a‡] Nan Li,[a] Shi Ming Zhou,[c] Hua Ming Sun,[a] Shi Wei Yin,[a] Na Zhao*[a] and Ben Zhong Tang*[b]

Organic solid fluorophores with tunable emission color have been widely applied in multiple areas. However, rational design and efficient crafting of these fluorophores from the simple core skeleton is still a formidable challenge because of the undesirable concentration quenching emission effect. Herein, we present the development of two series of organic solid fluorophores based on the backbone of p-bis(2,2-dicyanovinyl)benzene. Notably, the introduction of either non-aromatic or aromatic substituents both provide fluorophores with a tunable emission color. Moreover, fluorophores with aromatic substituents exhibit additional unique optical phenomena, such as aggregation-induced emission, polymorphism-dependent emission, and reversible mechanochromic luminescence.

Introduction

Organic solid fluorophores that exhibit intense and tunable emission, particularly those with an emission across the whole visible spectrum, have received much attentions owing to their extensive application in the fabrication of organic light-emitting diodes (OLED),[1] optical devices,[2] organic luminescent displays,[3] and fluorescent sensors.[4] However, the traditional organic fluorophores are usually weakly or even non-emissive in the solid state, which is attributed to the inherent strong intermolecular π-π stacking interaction that consumes the excitation energy.[5] Averting this thorny aggregation-caused quenching (ACQ) process is the key to obtaining organic solid fluorophores with superior optical properties. During the past decade, the discovery of a novel phenomenon, termed aggregation-induced emission (AIE) with the mechanism of restriction of intramolecular rotation (RIR), has provided new insight and powerful tools for the construction of organic solid fluorophores with immunity to the ACQ process.[6-7] To date, numerous elegant organic solid emitters based on diverse core skeletons have emerged that exhibit the AIE effect, and extensive technological applications have been developed.[8] However, the AIE system with a tunable emission color based on a simple core backbone is still extremely rare.[9]

Recently, extended π-conjugated molecules with D-π-A structure have attracted significant interest because of their flexibility in creating organic emitters with tunable emission.[10-11] The nitrile group, due to its strong electron-withdrawing ability and structural simplicity, is an ideal candidate as an excellent acceptor for such D-π-A fluorescent materials featuring advanced photoluminescent properties. More importantly, the nitrile group can induce steric hindrance and result in a twisted conformation which enables the fluorophores to prevent from the ACQ effect.[12] However, studies on regulating the emission behavior of a nitrile-containing system through altering the substituents are rare.[9] Herein, we present the development of two series of symmetric p-bis(2,2-dicyanovinyl)benzene-based fluorophores by decorating the single benzene ring with dicyanovinyl unit as acceptor and different types of donor with diverse electronic and steric effects (Fig. 1). Interestingly, with the introduction of either non-aromatic or aromatic substituents, both classes of fluorophores yield a full-color emission. Moreover, the aromatic groups can successfully endow the fluorophores with high efficient solid state emission and AIE effect. Meanwhile, specific polymorphism-dependent emission as well as mechanochromic luminescence are observed for some AIE fluorophores.
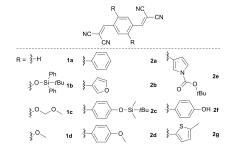

Fig. 1 Chemical structures of **1a**-**2g**.

a. Key Laboratory of Macromolecular Science of Shaanxi Province and School of Chemistry & Chemical Engineering, Shaanxi Normal University, Xi'an, 710119, China. E-mail: nzhao@snnu.edu.cn.
b. Department of Chemistry, The Hong Kong University of Science and Technology, Clear Water Bay, Kowloon, Hong Kong, China. E-mail: tangbenz@ust.hk.
c. Hefei National Laboratory for Physical Sciences at the Microscale, University of Science and Technology of China, Hefei, 230026, China.
†Electronic Supplementary Information (ESI) available: Synthesis and characterization, optical spectra, crystal data and DFT calculations. See DOI: 10.1039/x0xx00000x
‡These authors contributed equally to this work.

Results and discussion

The initial step of our research was to merge the components of both donor and acceptor into the desired compounds **1a–2g**. This was readily achieved by a one-step condensation reaction between the appropriate aldehydes and malononitrile. All compounds were easily purified by column chromatography or recrystallization with a reasonable yield.

The absorption and photoluminescence properties of all compounds in acetone and the solid state are shown in Table 1, as well as Figs. S1-2. For parent compound **1a**, the longest absorption peak was located at around 367 nm, which is ascribed to the π-π* transition. When the substitute group at 2,5-position was altered from *t*-butyldiphenylsiloxyl to methoxyl (or from aromatic phenyl to 5-methylthienyl), the corresponding **1b–1d** (or **2a–2g**) exhibited the longest absorption peak ranging from 428 to 457 nm (or 392 to 441 nm), which is assigned to the intramolecular charge transfer (ICT) transition from the different types of electron-donating group to electron-accepting dicyanovinyl group.[10]

As shown in Table 1, with increasing of the electron-donating ability, the emission wavelength of **1a–1d** in acetone presented a red-shift from 426 to 562 nm. While the emission peak in the solid state ranged from 467 to 620 nm. By changing the substituent with the aromatic group, the emission peak of **2a–2g** in acetone varied from 495 to 600 nm. Additionally, a similar red shifted emission tendency (464 to 622 nm) in the solid state was observed. It is clear that two series of solid emitters over the entire color range were obtained by simply varying the types of donor (Fig. 2). The CIE chromaticity diagrams (Figs. S3–4, Table S3) demonstrate the same tunable emission color from blue CIE (0.1374, 0.0374) to red CIE (0.6954, 0.3045). Furthermore, single crystals for all compounds, except **1b** and **2f**, were obtained by slow evaporation from appropriate solvent (Tables S6–8, Fig. S5),[13] which also emitted fluorescence covering the whole visible region (464 to 640 nm for series **1** and 467 to 593 nm for series **2**).

Fig. 2 Normalized PL spectra of **1a–1d** and **2a–2g** in the solid state, and the photographs taken under irradiation of 365 nm UV light.

To better understand the transition of all compounds, the density functional theory (DFT) calculations, using the single crystal structure determined by X-ray analysis, were carried out (Table S1). The results indicated that both the highest occupied molecular orbital (HOMO) and the lowest unoccupied molecular orbital (LUMO) of **1a** were localized on the whole molecular framework, suggesting a π-π* transition. For other compounds, however, the HOMO was mainly located on the core benzene ring and electron-donating moieties, while the LUMO was delocalized primarily over the central benzene ring and the electron-withdrawing dicyanovinyl group, which demonstrated the existence of ICT character for those compounds. Meanwhile, the HOMO and LUMO became more separated in series **2**, compared with that in series **1,** which was ascribed to the twisted conformation of series **2** originating from the steric hindrance by the introduction of bulky aromatic group. The dipole moment change ($\Delta\mu$) between the excited state (μ_e) and ground state (μ_g) were also determined (Table S2).

Table 1. Optical properties of **1a–2g**.

Compound	Solution state					Solid (Crystalline) state		
	λ_{abs} [nm][a]	ε [×10³M⁻¹cm⁻¹]	λ_{em} [nm]	$\mathnormal{Ø}_F$ [%][b]	τ_{avg} [ns][c]	λ_{em} [nm]	$\mathnormal{Ø}_F$ [%][b]	τ_{avg} [ns] [c]
1a	367	31.12	426	0.8	1.10	467 (464)	13.2 (3.4)	2.05 (2.27)
1b	430	3.38	538	15.7	5.21	502	11.3	1.57
1c	428	10.66	550	55.9	7.31	570 (574)	2.4 (2.2)	2.46 (3.98)
1d	457	9.20	562	76.3	10.62	620 (640)	3.7 (4.8)	7.42 (7.36)
2a	393	4.74	495	11.9	2.95	464 (467)	13.3 (9.3)	0.92 (2.87)
2b	398	7.30	545	1.5	3.18	514 (527)	18.3 (6.5)	2.72 (1.64)
2c	409	2.90	566	0.4	0.81	533 (538)	45.6 (53.8)	8.21 (8.06)
2d	418	4.60	565	0.9	1.81	545 (545/560)[e]	13.1 (49.0/7.9)[e]	6.27 (6.29/3.89)[e]
2e	415	6.40	n.d.[d]	0.5	n.d.[d]	566 (570)	35.6 (43.1)	7.33 (10.75)
2f	421	5.30	n.d.[d]	0.2	n.d.[d]	584	2.3	0.55
2g	441	3.00	600	3.9	1.75	622 (593)	11.7 (21.2)	4.16 (4.90)

[a] Longest wavelength absorption maximum in acetone. [b] Absolute fluorescence quantum yield measured by using the calibrated integrating sphere system. [c] Mean fluorescence lifetime (τ_{avg}) calculated by using the equation $\tau_{avg} = A_1\tau_1 + A_2\tau_2$. [d] Under detection limit. [e] two types (**2d-y/2d-o**) of crystal **2d**.

Journal Name

ARTICLE

The results showed the $\Delta\mu$ value for series **2** was larger than that of series **1**, which was in agreement with the degree of separation between the HOMO and LUMO. Furthermore, **1b**–**2g** exhibited an obvious solvent effect (Figs. S6–7).[14] With increasing of the solvent polarity (from cyclohexane to acetone or dichloromethane), the emission peak exhibited a red-shift, which indicated the existence of ICT in these compounds. However, slight solvent effect was observed for **1a**, confirming its π-π* character.

The fluorescence quantum yields (Φ_F) of all compounds in solution and the solid state (including crystal) are also summarized in Table 1. The quantum yields of **1b**–**1d** dissolved in acetone were moderate to high (15.7%–76.3%), but significantly decreased in the solid state (< 11.3% for solid powder, < 4.81% for crystal). In sharp contrast, a dramatic enhancement was achieved for **1a** and **2a**–**2g** in the solid state (2.3%–45.6% for solid powder, 3.4%–58.8% for crystal) compared with that in solution (0.2%–11.9%). It is noteworthy that **1d** and **2g** exhibited red emission. More importantly, **2g** retained a high quantum yield in the solid state (622 nm, 11.7%) and crystal (593 nm, 21.2%). Considering that red fluorophores containing π-conjugated framework typically have a tendency to aggregate in the solid form, which results in the emission quenching, this strategy provides an extremely powerful method to fabricate organic solid emitters with long emission wavelength. We also calculated the ratio of quantum yield between the solid and solution states to verify the influence of substitute group on the emission behavior of those compounds (Fig. 3D). It's clear that the ratio was over than one for **1a** and **2a**–**2g** but less than one for **1b**–**1d**. Therefore, the introduction of aromatic group successfully reversed the trend of the quantum yields between the solution and solid phases.

The higher quantum yield in the solid state implies the existence of the AIE effect. Therefore, we measured the AIE property using acetone and water to serve as good and poor solvent, respectively. Typically, **2e** was almost non-emissive when dissolved in acetone. An increase of water fraction (f_w) resulted in a significant boost of the emission intensity at 576 nm, and yielded approximately 150-fold enhancement when f_w was up to 99% (Figs. 3A–B). The observed phenomenon could be attributed to the aggregation of molecules formed in the mixed solution with high f_w, and thus activation of the RIR process. The particle size of **2e** in the mixture with f_w of 99% was determined to be 84 nm by dynamic light scattering (DLS), confirming the formation of the nano-aggregates (Fig. 3C). Furthermore, other compounds in series **2** and **1a** also displayed similar AIE or aggregation-induced emission enhancement (AIEE) performance (Figs. S8, S12–17). Nevertheless, compounds **1b**–**1d** with non-aromatic moieties exhibited the opposite

phenomenon, where an increase of the water fraction resulted in a gradual decrease of the emission intensity, suggesting their ACQ property (Figs. S9–11).
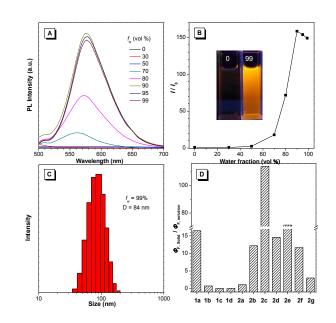

Fig. 3 (A) PL spectra of **2e** (10 μM) in acetone and acetone/water mixtures with different water fractions (f_w). (B) Plots of the emission intensity *versus* the composition of the water mixtures of **2e**. (C) Particle size distribution of **2e** (10 μM) in acetone/water mixtures with f_w values of 99%. (D) The ratio of the quantum yield between the solid and solution state of all compounds. Inset in B: photograph of **2e** in acetone/water mixtures with f_w values of 0 and 99% under irradiation of 365 nm UV light.

The fluorescence lifetime (τ) of all compounds are listed in Table 1 and Table S4. To verify the photoemission dynamics, the radiative transition rate constants (k_r) as well as nonradiative transition rate constants (k_{nr}) were calculated by using the fluorescence lifetime and quantum yields (Table S5). Taking **1d** as an example, k_{nr} (2.232×10^7 s^{-1}) was close to k_r (7.185×10^7 s^{-1}) in solution. However, k_{nr} was enhanced to 1.297×10^8 s^{-1} while k_r was reduced to 4.986×10^6 s^{-1} in the solid state, implying that nonradiative decay was dominant in the solid state. Whereas for **2c**, k_{nr} (1.229×10^9 s^{-1}) was remarkably greater than k_r (4.938×10^6 s^{-1}) in solution. However, k_{nr} was decreased to 6.626×10^7 s^{-1} while k_r was enhanced to 5.554×10^7 s^{-1} in the solid state. These results suggested that suppression of nonradiative decay was the major reason for the higher quantum yield in the solid state.

To gain the underlying reasons for this significant substituent dependent emission behavior, single crystal inspection was performed. Fig. 4 presents the single crystals of **1d** and **2c** as examples. Crystal **1d** adopted a near-planar conformation and

the torsion angle between vinyl (or methyl) group and the central phenyl ring was merely 3.42° (or 3.63°). Carefully evaluating the details of the crystal packing indicated that the distance between two adjacent planes was 3.416 Å, which suggested that **1d** encountered strong and consecutive intermolecular π-π stacking interaction and thus resulted in the weakening of fluorescence in the solid state (Fig. 4A).[15] A similar strong π-π stacking interaction (3.214 Å) was also observed for crystal **1c** (Fig. S21B), and was responsible for its reduced fluorescence in the solid state. In contrast, the crystal **2c** clearly showed a contorted conformation, where the torsion angle between vinyl (or substituted phenyl) group and the central benzene ring was 42.14° (or 40.15°), which apparently results from the steric congestion between the neighboring phenyl rings and dicyanovinyl moieties. Such twisted conformation effectively enlarged the distance between adjacent phenyl group (> 4.076 Å), and avoided the typical π-π stacking interaction (Fig. 4B). Meanwhile, crystallographic analyses of other compounds in series **2** declared similar twisted conformation and absence of π-π stacking interaction, which accounted for their bright luminescence in the solid state (Figs. S22–24). Compared with the other molecular packing in series **2,** it's clear that introduction of the bulky substituent did not enlarge the distance between adjacent molecules, implying the relatively tight packing of crystal **2c** and **2e**. Additionally, multiple intermolecular C–H···N (or C–H···O) and C–H···π interaction have been found throughout the crystal structure of **2c** and **2e** (Figs. S25, S23A), which could help rigidify the molecular conformation, hence, resulted in their relatively high emission efficiency in the solid state. It is interesting to note that there was also no π-π stacking interaction in crystal **1a**, though it exhibited an almost planar conformation (Fig. S21A), which leaded to no emission quenching in the solid state.
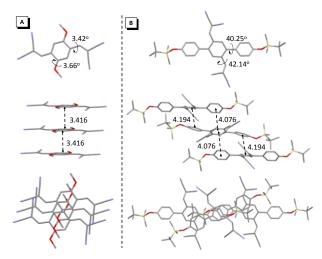

Fig. 4 Single crystal structure of **1d** (A) and **2c** (B), and molecular packing viewed from side and top of the adjacent molecules.

Unexpectedly, two types of **2d** with crystallographically independent conformations (**2d-g** and **2d-o**) suitable for X-ray analysis were obtained from its ethyl acetate/dichloromethane and ethyl acetate/acetone mixtures. The crystal **2d-g** exhibited green emission at around 545 nm, while the **2d-o** showed a bathochromic shift with orange emission at 560 nm (Fig. 5A). Both **2d-g** and **2d-o** adopted highly twisted conformations without π-π stacking interaction (Fig. S24). The most pronounced difference between the two forms were the dihedral angles between dicyanovinyl unit and 4-methoxyl phenyl moiety, which was 46.27° for **2d-g** and 43.06° for **2d-o**, respectively (Fig. 5B). This difference indicated that the conformation of **2d-o** was more planer than that of **2d-g**, thus endowed **2d-o** with a longer emission wavelength. Moreover, the two crystals presented entirely different packing mode (Figs. 5C–5D) and the amount of intermolecular C–H···N interactions between cyano and phenyl or methyl group in **2d-g** was more than that in **2d-o** (Fig. S24), enabling **2d-g** to possess higher quantum yield.
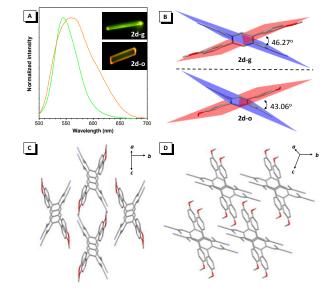

Fig. 5 (A) PL spectra of **2d-g** and **2d-o**. (B) The view of dihedral angles for **2d-g** and **2d-o**. Molecular packing in **2d-g** (C) and **2d-o** (D). Inset in A: photographs of **2d-g** and **2d-o** under a fluorescence microscope.

It is noted that as-prepared sample **2d** exhibited an emission peak at 545 nm, which was close to that of **2d-g**. However, gentle grinding induced a red-shift of the emission to 567 nm, which could be ascribed to the amorphous form of **2d** (Fig. 6A). Such amorphous state was further confirmed by its flat signal from the powder XRD measurement (Fig. S20B). Meanwhile, the red-shifted emission could be attributed to the collapse of the crystalline lattice by grinding, which resulted in the molecules adopting a more planar conformation. One of the apparent phenomena is that amorphous solid can always be crystallized by either heating or fuming with an organic solvent vapor.[16] Indeed, this was also applicable for **2d** (Fig. 6B). While fuming with the dichloromethane vapor, the amorphous form of **2d** was converted into the crystalline form with the emission peak restored to 545 nm. Moreover, this process could be repeated several times, indicating the reversible mechanochromic luminescence property of **2d** in response to external stimuli. A similar reversible emission behavior for as-prepared powders of **2b** and **2c** could also be achieved by a repeated grinding/solvent fuming process (Figs. S18–19).
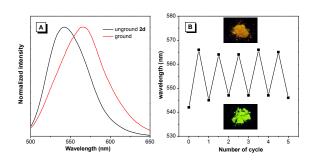
Fig. 6 (A) PL spectra of unground and ground **2d**. (B) Reversible switching of the emission of **2d** by repeated grinding/fuming cycles. Inset in B: photographs of as-prepared **2d** and after grinding under 365 nm irradiation.

Conclusions

In conclusion, two classes of *p*-bis(2,2-dicyanovinyl)benzene-based fluorophores were designed and synthesized. Their optical properties, as well as single crystal packing structures, were systematically investigated. The results showed that decorating with either non-aromatic or aromatic groups at the core backbone generated two kinds of organic solid emitters with tunable emission from the blue to red regions. More importantly, the employment of bulky aromatic groups successfully resulted in the twisted molecular conformation. Such contorted conformation was beneficial for the inhibition of detrimental π-π stacking interaction and assisted the fluorophores to exhibit remarkable AIE feature with high emission efficiency in the solid state. In addition, some AIE fluorophores presented polymorphism-dependent emission and reversible mechanochromic luminescence property. Since these fluorophores exhibiting diverse emission characteristics are all derivatives of a single benzene ring, we believe such strategy provides a rational and efficient approach for the fabrication of novel organic solid fluorophores from both fundamental and practical viewpoints.

Acknowledgements

Notes and references

1   (a) L. Duan, J. Qiao, Y. Sun and Y. Qiu, *Adv. Mater.*, 2011, **23**, 1137-1144; (b) R. H. Friend, R. W. Gymer, A. B. Holms, J. H. Burroughes, R. N. Marks, C. Taliani, D. D. C. Bradley, D. A. Dos Santos, J. L. Brédas, M. Lögdlund and W. R. Salaneck, *Nature*, 1999, **397**, 121-128; (c) A. C. Grimsdale, K. L. Chan, R. E. Martin, P. G. Jokisz and A. B. Holmes, *Chem, Rev.*, 2009, **109**, 897-1091; (d) T. Qin, W. Wiedemair, S. Nau, R. Trattnig, S. Sax, S. Winkler,

A. Vollmer, N. Koch, M. Baumgarten, E. J. W. List, K. Müllen, *J. Am. Chem. Soc.*, 2011, **133**, 1301-1303.

2   J. Zhang, W. Chen, J. A. Rojas, V. E. Jucov, V. T. Timofeeva, C. T. Parker, S. Barlow and R. S. Marder, *J. Am. Chem. Soc.*, 2013, **135**, 16376-16379.

3   T. Weil, T. Vosch, J. Hofkens, K. Peneva and K. Müllen, *Angew. Chem. Int. Ed.*, 2010, **49**, 9068-9093.

4   (a) S. W. Thomas III, G. D. Joly and T. M. Swager, *Chem. Rev.*, 2007, **107**, 1339-1386; (b) A. P. de Silva, H. Q. N. Gunaratne, T. Gunnlaugsson, A. J. M. Huxley, C. P. McCoy, J. T. Rademacher and T. E. Rice, *Chem. Rev.*, 1997, **97**, 1515-1566; (c) L. Basabe-Desmonts, D. N. Reinhoudt and M. Crego-Calama, *Chem. Soc. Rev.*, 2007, **36**, 993-1017.

5   (a) G. S. Beddard and G. Porter, *Nature*, 1976, **260**, 366-367; (b) Y. Hong, J. W. Y. Lam and B. Z. Tang, *Chem. Commun.*, 2009, 4332-4353; (c) C.-K. Lim, S. Kim, I. C. Kwon, C.-H. Ahn and S. Y. Park, *Chem. Mater.*, 2009, **21**, 5819-5825.

6   (a) J. Luo, Z. Xie, J. W. Y. Lam, L. Cheng, H. Chen, C. Qiu, H. S. Kwok, X. Zhan, Y. Liu, D. Zhu and B. Z. Tang, *Chem. Commun.*, 2001, 1740-1741; (b) B.-K. An, S.-K. Kwon, S.-D. Jung and S. Y. Park, *J. Am. Chem. Soc.*, 2002, **124**, 14410-14415.

7   (a) J. Chen, C. C. W. Law, J. W. Y. Lam, Y. Dong, S. M. F. Lo, I. D. Williams, D. Zhu and B. Z. Tang, *Chem. Mater.*, 2003, **15**, 1535-1546; (b) G. Yu, S. Yin, Y. Liu, J. Chen, X. Xu, X. Sun, D. Ma, X. Zhan, Q. Peng, Z. G. Shuai, B. Z. Tang, D. B. Zhu, W. Fang and Y. Luo, *J. Am. Chem. Soc.*, 2005, **127**, 6335-6346; (c) J. Mei, Y. Hong, J. W. Y. Lam, A. Qin and B. Z. Tang, *Adv. Mater.*, 2014, **26**, 5429-5479.

8   (a) J. Mei, N. L. C. Leung, R. T. K. Kwok, J. W. Y. Law and B. Z. Tang, *Chem. Rev.*, 2015, **115**, 11718-11940; (b) S. Xu, T. Liu, Y. Mu, Y. F. Wang, Z. Chi, C. C. Lo, S. Liu, Y. Zhang, A. Lien and J. Xu, *Angew. Chem. Int. Ed.*, 2015, **54**, 874-878; (c) S.-J. Yoon, J. W. Chung, J. Gierschner, K. S. Kim, M.-G. Choi, D. Kim and S. Y. Park, *J. Am. Chem. Soc.*, 2010, **132**, 13675-13683; (d) Y. Okazawa, K. Kondo, M. Akita and M. Yoshizawa, *J. Am. Chem. Soc.*, 2015, **137**, 98-101; (e) T. Shiragami, Y. Nakamura, J. Matsumoto, M. Otsuki and M. Yasuda, *Phys. Chem. Chem. Phys.*, 2014, **16**, 22046-22051; (f) X. Wang, J. Hu, G. Zhang and S. Liu, *J. Am. Chem. Soc.*, 2014, **136**, 9890-9893; (g) J. Zhang, B. Xu, J. Chen, S. Ma, Y. Dong, L. Wang, B. Li, L. Ye and W. Tian, *Adv. Mater.*, 2014, **26**, 739-745; (h) R. Yoshii, A. Hirose, K. Tanaka and Y. Chujo. *J. Am. Chem. Soc.*, 2014, **136**, 18131-18139; (i) S. Xu, Y. Yuan, X. Cai, C. J. Zhang, F. Hu, J. Liang, G. Zhang, D. Q. Zhang and B. Liu, *Chem. Sci.*, 2015, **6**, 5824-5830; (j) L. Peng, Y. Zheng, X. Wang, A. J. Tong and Y. Xiang, *Chem. Eur. J.*, 2015, **21**, 4326-4332; (k) J. Huang, N. Sun, Y. Dong, R. Tang, P. Lu, P. Cai, Q. Q. Li, D. Ma, J. Qin and Z. Li, *Adv. Funct. Mater.*, 2013, **23**, 2329-2337; (l) G. Chen, W. Li, T. Zhou, Q. Peng, D. Zhai, H. Li, W. Z. Yuan, Y. M. Zhang and B. Z. Tang, *Adv. Mater.*, 2015, **27**, 4496-4501; (m) M. Huang, R. Yu, K. Xu, S. Ye, S. Kuang, X. Zhu and Y. Wan, *Chem. Sci.*, 2016, **7**, 4485-4491.

9   (a) Z. Zhang, B. Xu, J. Su, L. Shen, Y. Xie and H. Tian, *Angew. Chem. Int. Ed.*, 2011, **50**, 11654-11657; (b) S. P. Anthony, *ChemPluschem*, 2012, **77**, 518-531.

10 (a) Z. R. Grabowski, K. Rotkiewicz and W. Rettig, *Chem. Rev.*, 2003, **103**, 3899-4032; (b) C. T. Chen, *Chem. Mater.*, 2004, **16**, 4389-4400.

11 (a) A. Wakamiya, K. Mori and S. Yamaguchi, *Angew. Chem. Int. Ed.*, 2007, **46**, 4273-4276; (b) M. Shimizu, Y. Takeda, M. Higashi and T. Hiyama, *Angew. Chem. Int. Ed.*, 2009, **48**, 3653-3656; (c) E. Kim, Y. Lee, S. Lee and S. B. Park, *Acc. Chem. Res.*, 2015, **48**, 538-547; (d) A. C. Shaikh, D. S. Ranade, S. Thorat, A. Maity, P. P. Kulkarni, R. G. Gonnade, P. Munshi and N. T. Patil, *Chem, Commun.*, 2015, **51**, 16115-16118; (e) Z. Song, W. Zhang, M. Jiang, H. H. Y. Sung, R. T. K. Kwok, H. Nie, I. D. Williams, B. Liu and B. Z. Tang, *Adv. Funct. Mater.*, 2016, **26**, 824-832.

Chemical Science Accepted Manuscript

12 (a) K. A. N. Upamali, L. A. Estrada, P. K. De, X. Cai, J. A. Krause and D. C. Neckers, *Langmuir*, 2011, **27**, 1573-1580; (b) B.-K. An, J. Gierschner and S. Y. Park, *Acc. Chem. Res.*, 2012, **45**, 544-554; (c) E. Ishow, A. Brosseau, G. Clavier, K. Nakatani, P. Tauc, C. Fiorini-Debuisschert, S. Neveu, O. Sandre and A. Léaustic, *Chem. Mater.*, 2008, **20**, 6597-6599.

13 CCDC 1056239 (**1a**), 1056280 (**1c**), 1403124 (**1d**), 1439334 (**2a**), 1439332 (**2b**), 1443616 (**2c**), 1472574 (**2d-g**), 1499316 (**2d-o**), 1442948 (**2e**) and 1442404 (**2g**) contain the supplementary crystallographic data for this paper. These data are provided free of charge by the Cambridge Crystallographic Data Centre via www.ccdc.cam.ac.uk/data_request/cif.

14 The solvent effect of **2f** could not be measured due to its poor solubility.

15 M. D. Curtis, J. Cao and J. W. Kampf, *J. Am. Chem. Soc.*, 2004, **126**, 4318-4328.

16 (a) Z. He, L. Zhang, J. Mei, T. Zhang, J. W. Y. Lam, Z. Shuai, Y. Q. Dong and B. Z. Tang, *Chem. Mater.*, 2015, **27**, 6601-6607; (b) Y. Sagara and T. Kato, *Nat. Chem.*, 2009, **1**, 605-610; (c) K. Nagura, S. Saito, H. Yusa, H. Yamawaki, H. Fujihisa, H. Sato, Y. Shimoikeda and S. Yamaguchi, *J. Am. Chem. Soc.*, 2013, **135**, 10322-10325; (d) C. Dou, L. Han, S. Zhao, H. Zhang and Y. Wang, *J. Phys. Chem. Lett.*, 2011, **2**, 666-670; (e) H. Naito, Y. Morisaki and Y. Chujo, *Angew. Chem. Int. Ed.*, 2015, **54**, 5084-5087; (f) M.-S. Yuan, D.-E. Wang, P. Xue, W. Wang, J.-C. Wang, Q. Tu, Z. Liu, Y. Liu, Y. Zhang and J. Wang, *Chem. Mater.*, 2014, **26**, 2467-2477; (g) Z. Chi, X. Zhang, B. Xu, X. Zhou, C. Ma, Y. Zhang, S. Liu and J. Xu, *Chem. Soc. Rev.*, 2012, **41**, 3878-3896.